Initial Rotor Position Estimation for Wound-Rotor Synchronous Starter/Generators Based on Multi-Stage-Structure Characteristics

Tao Meng, Weiguo Liu, Ningfei Jiao, Jichang Peng and Yujie Zhu
Shaanxi Key Laboratory of Small & Special Electrical Machine and Drive Technology
Department of Electrical Engineering, Northwestern Polytechnical University
Xi'an, Shaanxi 710072, P. R. China
Emails: mengtao0504@gmail.com, jiaoningfei@gmail.com, lwglll@nwpu.edu.cn, linkpjc@gmail.com, 18710395673@126.com

***Abstract*—The inductance parameters of the main generator of a wound-rotor synchronous starter/generator changed significantly with the variation of field current and armature current, so traditional position estimation methods based on magnetic saliency are no longer applicable. In order to improve the accuracy of estimation, a novel initial rotor position estimation method of a wound-rotor synchronous starter/generator based on multi-stage-structure characteristics is proposed in this paper. Square wave voltage signals were imposed on the stator of the main generator, and the response current signals extracted on the stator of the main exciter were used to estimate position information. This method eliminates the dependency on the magnetic saliency. Experimental results verified the feasibility and effectiveness of this method.**

Keywords—wound-rotor synchronous starter/generator (WRSSG); initial rotor position estimation; multi-stage-structure characteristics; Square wave voltage

I. INTRODUCTION

In traditional aircraft propulsion and power system, the dedicated starter is only used to start the aero engine, whose utilization is particularly low. With the development of the more/all electric aircraft, there is an increasing demand of integrated starter/generator (ISG) system[1-3]. In the start-up process, the ISG act as a starter to start the aero engine. And then act as a generator to provide the power to the electrical equipment. The ISG system has smaller volume and lighter weight.

As a generator, the wound-rotor synchronous machine (WRSM) has the advantages of high reliability, adjustable power factor, and so on. Integrated starter/generator (ISG) system based on the WRSM is becoming increasingly popular in modern aircrafts. The structure of the WRSM with a two-phase brushless exciter is shown in Fig. 1. In the starting mode, the Pre-Exciter (PE) is not in working condition. And the two-phase field winding of the Main Exciter (ME) is supplied with two-phase AC excitation (in low speed region) or DC excitation (in high speed region) by the two-phase ME controller. Then the armature winding of the ME provides DC field current for the Main Generator (MG) through the rotating rectifier. The research on the ISG system based on a WRSM mainly focused on construction design[4] and start control technology[5-8].

This work was supported by National Natural Science Foundation of China (51677152).

In order to achieve the starting function for a WRSM, accurate rotor position information is required. Rotor position information is usually obtained by a rotating transformer or a photoelectric encoder, which is fixed on the same rotation shaft with the machine. As the traditional mechanical position sensor is facing the strict restrictions such as electromagnetic and space environment, the researchers have carried out the research on the initial position detection of the WRSM without position sensor. Pulsating high-frequency voltage signals were imposed on the MG stator winding in same interval electric angles to estimate the initial position in [9]. It depends on the machine saliency. In order to improve the accuracy of estimation results, the last response current should be return to zero before the next pulse signal voltage imposed on the stator terminal. Current signals of the ME and MG were used independently for position estimation in [10], but the simulation and experimental results were not shown in this paper. The induced armature electromotive forces due to the pulsation in the field current were used to detect the rotor position[11]. A new sensorless algorithm for electrically energized synchronous motor was proposed in [12] where the carrier signal was injected to the field winding. The method presented in [13] used the stator as the

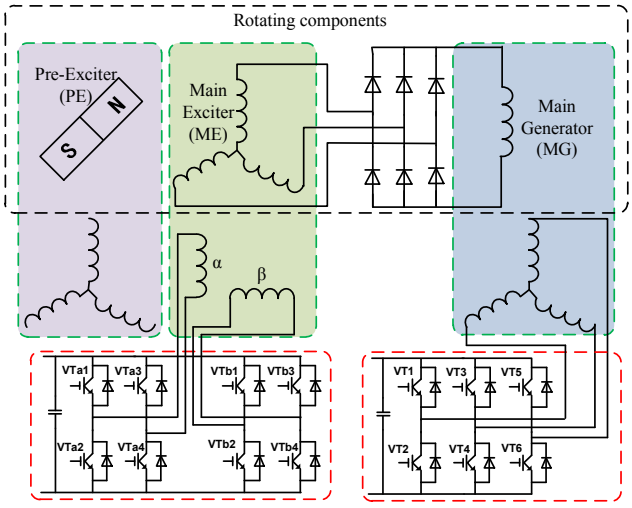

Fig. 1. Structure of the wound-rotor synchronous starter/generator with a two-phase brushless exciter.

transmitter and the rotor as the receiver of an alternating carrier signal to track the position.

In this paper, a novel initial rotor position estimation method based on the multi-stage-structure characteristics of the WRSSG is discussed. The mutual inductance between the MG stator windings and filed winding is considered in the proposed method, and the dependency on the magnetic saliency can be eliminated. A new signal transmission and detection channel between the MG and ME is established. It's a new signal process method with 'MG injection-ME detection', which is different from the traditional methods with 'MG injection-MG detection'.

II. Initial Rotor Position Estimation Principle Based on Multi-Stage-Structure Characteristics

The new transmission and detection channel with 'MG injection-ME detection' is shown in Fig. 2. When the square wave voltage signals are injected in the stator windings of MG, the response current signals extracted on the stator windings of the ME can be used to estimate initial rotor position of the MG.

This method includes two steps: A) high-frequency voltage signals are injected to the stator windings of MG to estimate the rotor position. B) low-frequency voltage signals are injected to the stator windings of MG to identify the quadrant.

A. Initial Rotor Position Estimated

The stator fundamental currents of the ME ignored the influence of the rotating rectifier are obtained as in (1).

$$\begin{cases} i_{es\alpha} = I_{em} \sin \omega_e t \\ i_{es\beta} = I_{em} \sin(\omega_e t + 90^\circ) \end{cases} \tag{1}$$

Where $i_{es\alpha}$ and $i_{es\beta}$ are α-/β-phase current, ω_e is the frequency of the current in radians per second, I_{em} is the amplitude of the fundamental current.

Firstly, high-frequency square wave voltage as shown in (2) is injected to α-axis of the stator of MG.

$$V_h = \begin{cases} V_h & , \quad (0, 0.5T_h] \\ -V_h & , \quad (0.5T_h, T_h] \end{cases} \tag{2}$$

where V_h and $\omega_h = 2\pi/T_h$ is the magnitude and frequency in radians per second of the injected signal, respectively. The

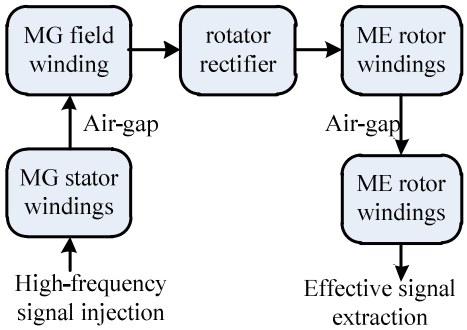

Fig. 2. Transmission and detection channel with 'MG injection-ME detection'

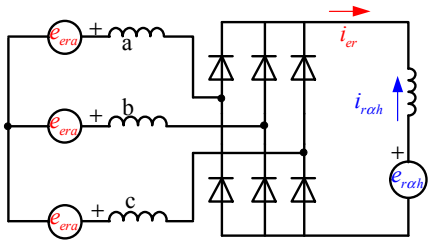

Fig. 3. Equivalent circuit of rotating components

frequency of the injected signal, ω_h, should be large enough compared to ω_e.

The equivalent circuit of rotating components of the WRSSG is shown in Fig. 3. i_{er} and $i_{r\alpha h}$ are fundamental current and high-frequency current, respectively.

When the high-frequency voltage injected into stator of the MG, the induced voltage in the field winding of the MG can be obtained as in (3).

$$e_{r\alpha h} = \begin{cases} E_{mh} \cos\theta_r & , \quad (0, 0.5T_h] \\ -E_{mh} \cos\theta_r & , \quad (0.5T_h, T_h] \end{cases} \tag{3}$$

where θ_r is the rotor position of the MG, E_{mh} is the magnitude of the induced voltage when $\theta_r = 0$.

As shown in Fig. 3, $i_{r\alpha h}$ is the current produced by $e_{r\alpha h}$ applied alone to the equivalent circuit. $i_{r\alpha h}$ should be not too big to provoke variation in torque that can be generated by MG. However, it is difficult to extract the effective rotor position information when $i_{r\alpha h}$ is too small. So the magnitude of the high-frequency voltage, V_h, should be selected appropriately.

Due to the usually very large electrical time constant of the field winding of the MG, high-frequency current produced by induced square voltage in field winding of the MG can be obtained approximately as in (4),

$$i_{r\alpha h} = I_{mh} \sin(\omega_h t - 90^\circ) \cos\theta_r \tag{4}$$

where I_{mh} is the magnitude of the current, $i_{r\alpha h}$, when $\theta_r = 0$.

The space phasor of the rotor fundamental currents of the ME is a hexagon[14]. As $i_{er} >> i_{r\alpha h}$, we assume that the rectifier works in normal states, the amplitude envelope of the high frequency currents space phasor in the ME rotor can be obtained as a hexagon, and the average angular velocity is ω_e.

From (4) and Fig. 3, the high-frequency induced currents in two-phase ME stator windings can be derived approximately as in (5)

$$\begin{cases} i_{es\alpha\alpha h} = I'_{mh} \sin(\omega_h t - 90^\circ) \cos\theta_r \sin\omega_e t \\ i_{es\beta\alpha h} = I'_{mh} \sin(\omega_h t - 90^\circ) \cos\theta_r \sin(\omega_e t + 90^\circ) \end{cases} \tag{5}$$

where I'_{mh} is the magnitude of the ME stator induced high frequency current.

From (1) and (5), the total currents of α-/β-phase of ME stator windings can be derived as in (6)

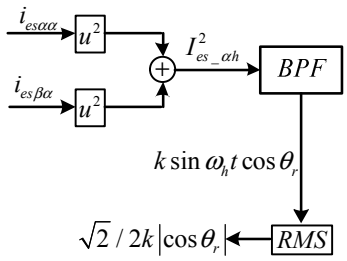

Fig. 4. Signal process to extract effective signal of rotor position

$$\begin{cases} i_{es\alpha\alpha} = i_{es\alpha\alpha h} + i_{es\alpha} \\ i_{es\beta\alpha} = i_{es\beta\alpha h} + i_{es\beta} \end{cases} \tag{6}$$

where $i_{es\alpha\alpha}$ and $i_{es\beta\alpha}$ are the currents obtained directly by the current sensors.

To extract effective signal of rotor position, a simple signal processing block can be used as shown in Fig. 4. The signal $I^2_{es\_\alpha h}$ is processed with the band-pass-filter (BPF) whose center frequency is same with the frequency of the injected signal, and then the cosine value of the rotor position, $\sqrt{2}/2k|cos\theta_r|$, is obtained.

Secondly, the same high-frequency square wave voltage as shown in (2) is injected to β-axis of the stator windings of MG. The induced voltage in the field winding of the MG and the corresponding high-frequency current are obtained as (7) and (8), respectively.

$$e_{r\beta h} = \begin{cases} E_{mh}\sin\theta_r & , \quad (0, 0.5T_h] \\ -E_{mh}\sin\theta_r & , \ (0.5T_h, T_h] \end{cases} \tag{7}$$

$$i_{r\beta h} = I_{mh}\sin(\omega_h t - 90^\circ)\sin\theta_r \tag{8}$$

In a similar way with the signal processing of α-axis injection from (4) ~ (6) and Fig. 4, the sine value of the rotor position, $\sqrt{2}/2k|sin\theta_r|$, is obtained.

Then, the estimated position value can be obtained as (9)

$$\left|\hat{\theta}_r\right| = \arctan((\sqrt{2}/2 * k|\sin\theta_r|)/(\sqrt{2}/2 * k|\cos\theta_r|)) \tag{9}$$

where, the symbol '| |' means that the quadrant information of the estimated rotor position is not clear.

Therefore, the following step deals with the identification of the quadrant of the rotor position.

B. Quadrant of the Rotor Position Identified

As mentioned above, the field winding of the MG has a very large electrical time constant. In order to avoid the identification error caused by time delay, low-frequency voltage is applied to the stator α/β-axis windings of the MG.

Firstly, low-frequency square wave voltage as shown in (10) is applied to α-axis of the stator of MG.

$$V_l = \begin{cases} V_l & , \quad (0, 0.5T_l] \\ -V_l & , \ (0.5T_l, T_l] \end{cases} \tag{10}$$

Where V_l and $\omega_l = 2\pi/T_l$ is the magnitude and frequency in radians per second of the injected signal, respectively.

The induced voltage in the field winding of the MG is obtained as in (11), and the low-frequency current in the field winding of the MG can be obtained as in (12)

$$e_{r\alpha l} = \begin{cases} E_{ml}\cos\theta_r & , \quad (0, 0.5T_l] \\ -E_{ml}\cos\theta_r & , \ (0.5T_l, T_l] \end{cases} \tag{11}$$

$$i_{r\alpha l} = \begin{cases} I_{ml}\cos\theta_r & , \quad (0, 0.5T_l] \\ -I_{ml}\cos\theta_r & , \ (0.5T_l, T_l] \end{cases} \tag{12}$$

where E_{ml} and I_{ml} are the amplitude of the low-frequency induced voltage and current, respectively, when $\theta_r = 0$.

It is noteworthy that The frequency of the injected signal, V_l, should be low enough to reduce the influence of large electrical time constant. The magnitude of the low frequency voltage should be an appropriate value. On one hand, it should be small enough to ensure the normal operation of the rotating rectifier. On the other hand, in order to identify the angel quadrant easily, $i_{r\alpha l}$, which is produced by V_l applied alone to the equivalent circuit as shown in Fig. 3, should not be too small.

Similarly to derivation process of (5), the low-frequency induced currents in ME stator windings can be derived approximately as in (13) and (14) from (12)

$$i_{es\alpha\alpha l} = \begin{cases} I'_{ml}\cos\theta_r\sin\omega_e t & , e_{r\alpha l} < 0 \\ -I'_{ml}\cos\theta_r\sin\omega_e t & , \text{ else} \end{cases} \tag{13}$$

$$i_{es\beta\alpha l} = \begin{cases} I'_{ml}\cos\theta_r\sin(\omega_e t + 90^\circ) & , e_{r\alpha l} < 0 \\ -I'_{ml}\cos\theta_r\sin(\omega_e t + 90^\circ) & , \text{ else} \end{cases} \tag{14}$$

where I'_{ml} is the magnitude of the induced current when $\theta_r = 0$.

The total currents of α-/β-phase of ME stator windings can be derived from (1), (13) and (14) as in (15).

$$\begin{cases} i_{es\alpha\alpha} = i_{es\alpha\alpha l} + i_{es\alpha} \\ i_{es\beta\alpha} = i_{es\beta\alpha l} + i_{es\beta} \end{cases} \tag{15}$$

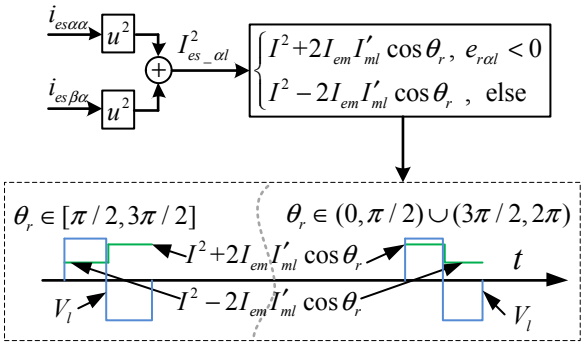

Fig. 5. The simple signal processing block and relationship between $I^2_{es\_\alpha l}$ and V_l

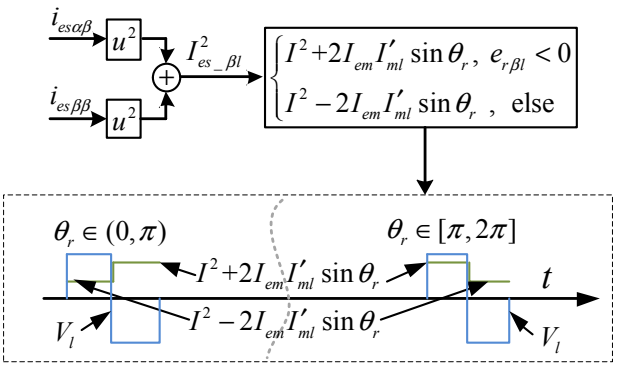

Fig. 6. The simple signal processing block and relationship between $I^2_{es\_\beta l}$ and V_l

TABLE I. THE RELATIONSHIP BETWEEN $\Delta I^2_{es\_\alpha l}$, $\Delta I^2_{es\_\beta l}$ AND QUADRANT

Position	Quadrant	$\Delta I^2_{es\_\alpha l}$	$\Delta I^2_{es\_\beta l}$
$(0,\pi/2)$	I	–	–
$(\pi/2,\pi)$	II	+	–
$(\pi,3\pi/2)$	III	+	+
$(3\pi/2,2\pi)$	IV	–	+

As a result of a simple signal processing block, the relationship between and is obtained as shown in Fig. 5. Where $I^2=I^2_{em}+(I'_{ml}cos\theta_r)^2$.

Secondly, the same low-frequency square wave voltage as shown in (10) is injected to β-axis of the stator windings of MG, and total currents of α-/β-phase of ME stator windings can be derived as in (16).

$$\begin{cases} i_{es\alpha\beta}=i_{es\alpha\beta l}+i_{es\alpha} \\ i_{es\beta\beta}=i_{es\beta\beta l}+i_{es\beta} \end{cases} \tag{16}$$

As a result of a simple signal processing block, the relationship between and is obtained as shown in Fig. 6. Where $I^2=I^2_{em}+(I'_{ml}sin\theta_r)^2$.

In order to show the relationship between the effective low frequency current and the quadrant more clearly, two symbols, $\Delta I^2_{es\_\alpha l}$ and $\Delta I^2_{es\_\beta l}$ are defined as in (17)

$$\begin{cases} \Delta I^2_{es\_\alpha l}=I^2_{es\_\alpha l\_+}-I^2_{es\_\alpha l\_-} \\ \Delta I^2_{es\_\beta l}=I^2_{es\_\beta l\_+}-I^2_{es\_\beta l\_-} \end{cases} \tag{17}$$

where $I^2_{es\_\alpha l\_+}$ is the average value of the current $I^2_{es\_\alpha l}$ when $V_l>0$, $I^2_{es\_\alpha l\_-}$ is the average value of the current $I^2_{es\_\alpha l}$ when $V_l<0$. So it is the same with $I^2_{es\_\beta l\_+}$ and $I^2_{es\_\beta l\_-}$. Then the relationship between $\Delta I^2_{es\_\alpha l}$ and $\Delta I^2_{es\_\beta l}$ and quadrant of the rotor position is obtained as in Table I.

When $\Delta I^2_{es\_\alpha l}=0$ or $\Delta I^2_{es\_\beta l}=0$, the relationship between $\Delta I^2_{es\_\alpha l}$ and $\Delta I^2_{es\_\beta l}$ and rotor position is shown in (18).

$$\theta_r=\begin{cases} 0 & ,\Delta I^2_{es\_\alpha l}<0\,\&\,\Delta I^2_{es\_\beta l}=0 \\ \pi/2 & ,\Delta I^2_{es\_\alpha l}=0\,\&\,\Delta I^2_{es\_\beta l}<0 \\ \pi & ,\Delta I^2_{es\_\alpha l}>0\,\&\,\Delta I^2_{es\_\beta l}=0 \\ 3\pi/2 & ,\Delta I^2_{es\_\alpha l}=0\,\&\,\Delta I^2_{es\_\beta l}>0 \end{cases} \tag{18}$$

III. EXPERIMENTAL RESULTS

Experiment platform, containing a starter/generator system and load platform, was built as shown in Fig. 7. The load platform was set at a constant torque value, which was the same with the real load. The control algorithms was implemented on the RTLAB real-time system. The sampling frequency was 20 kHz, and the pulse width modulation (PWM) switching frequency is 5 kHz.

The system configuration for the experiments is shown in Fig. 8. The single pole double throw switch, which just shows which axis of the MG the injection square voltage is applied to, is not a real mechanical switch. It is controlled by a timer in the control algorithms. The values $\sqrt{2}/2k|cos\theta_r|$, $\sqrt{2}/2k|sin\theta_r|$, $\Delta I^2_{es\_\alpha l}$ and $\Delta I^2_{es\_\beta l}$ obtained in different time are stored in the registers.

In the experiments, the magnitude and frequency of the high-frequency voltage signal are 20V and 1.25 kHz. The high-frequency signal is applied to the α- axis and β-axis windings of the MG stator successively. The currents collected from the ME

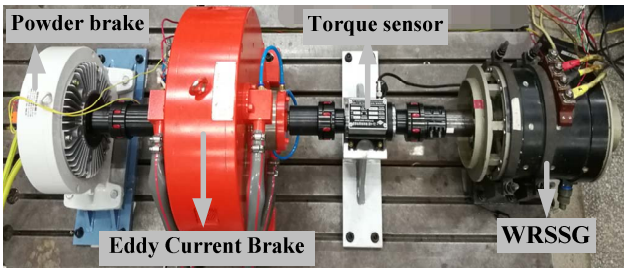

Fig. 7. Experiment platform

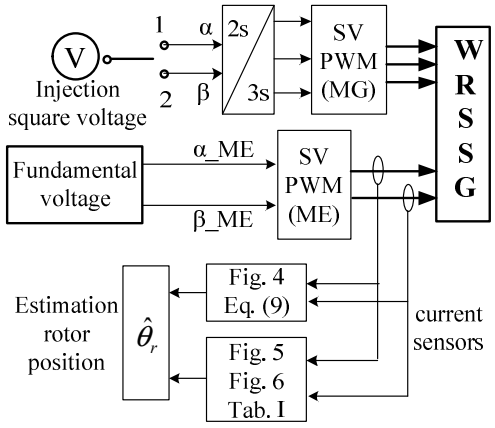

Fig. 8. System configuration for the experiments

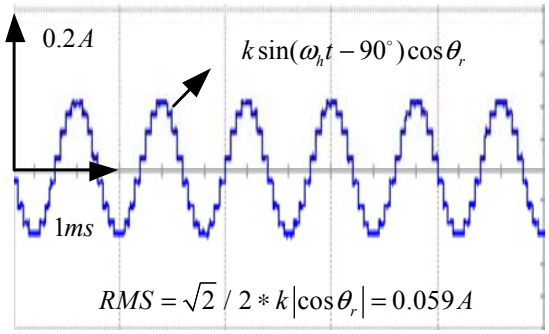

Fig. 9. Cosine signal with α-axis injected

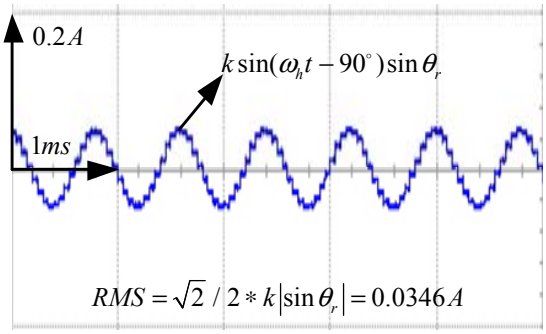

Fig. 10. Sine signal with β-axis injected

stator windings are processed by signal processing block as shown in Fig. 4. Then the cosine and sine signals of the rotor position are obtained as shown in Fig. 9 and Fig. 10. In order to reduce the influence of sampling error on calculation accuracy, the average root mean square (RMS) value of five periodic in the steady state as the final sine signal RMS.

The low-frequency voltage signal used to identify the quadrant are 12V and 10 Hz. The low-frequency signal is applied to the α-axis and β-axis windings of the MG stator successively. The currents collected from the ME stator windings with α-axis and β-axis injected are processed by signal processing block as shown in Fig. 5 and Fig. 6, respectively.

Finally, the estimated rotor position in different quadrants

TABLE II. THE ESTIMATED ROTOR POSITION IN DIFFERENT QUADRANTS

θ_r/rad	$\hat{\theta}_r$/rad	$\tilde{\theta}_r$/rad
0.5415	0.5301	0.0114
1.8285	1.7888	0.0397
3.4484	3.5053	-0.0569
5.303	5.3436	-0.0433

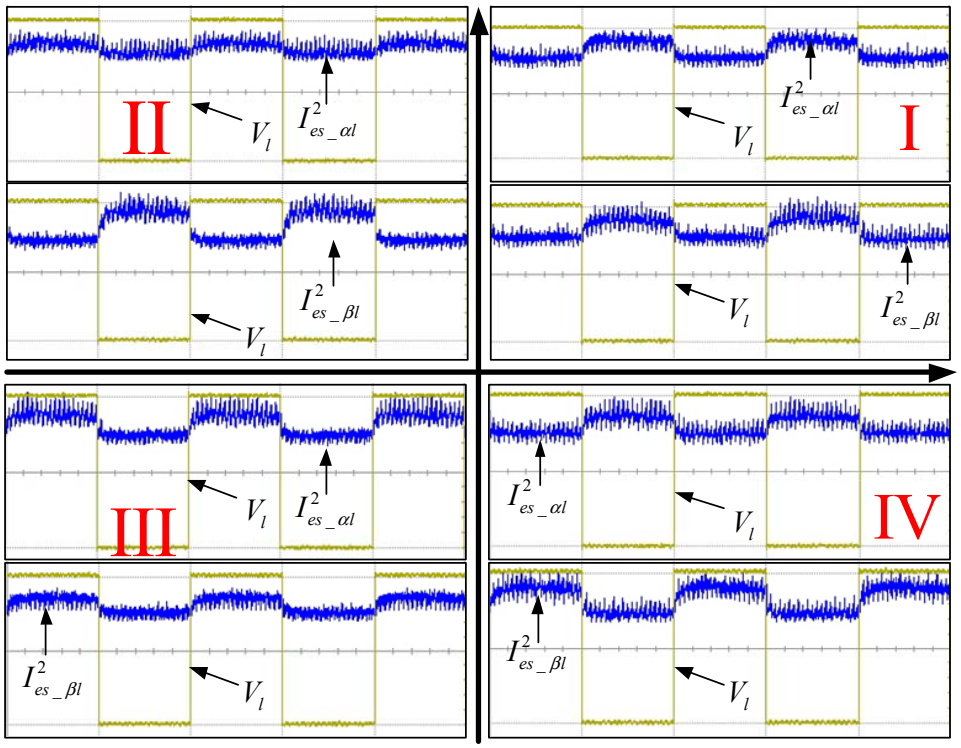

Fig. 11. The currents $I^2_{es\_\alpha l}$ and $I^2_{es\_\beta l}$ in different quadrants

are obtained as in Table II, and the currents $I^2_{es\_\alpha l}$ and $I^2_{es\_\beta l}$ in different quadrants are shown in Fig. 11. From Table II we can get that the estimated error is no more than 0.0569 rad (about 3 electrical degrees), which meets the precision requirements for the rotor initial position in the actual starting process of the WRSSG.

IV. CONCLUTION

In this paper, a new initial position estimation method for the wound-rotor synchronous starter/generator using square wave voltage signal injection based on multi-stage-structure characteristics has been proposed. The proposed method based on the principle that the mutual inductance varies with rotor position, and eliminates the dependency on the machine saliency. Experiment platform containing a WRSSG prototype was built, and the control algorithms was implemented on the RTLAB real-time system. The experimental results verified that the proposed method can obtain accurate estimation performance.

REFERENCES

[1] B. S. Bhangu and K. Rajashekara, "Electric Starter Generators: Their Integration into Gas Turbine Engines," Industry Applications Magazine, IEEE, vol. 20, pp. 14-22, 2014.

[2] C. A. Ferreira, S. R. Jones, W. S. Heglund, and W. D. Jones, "Detailed design of a 30-kW switched reluctance starter/generator system for a gas turbine engine application," Industry Applications, IEEE Transactions on, vol. 31, pp. 553-561, 1995.

[3] A. K. Jain, S. Mathapati, V. T. Ranganathan, and V. Narayanan, "Integrated starter generator for 42-V powernet using induction machine and direct torque control technique," Power Electronics, IEEE Transactions on, vol. 21, pp. 701-710, 2006.

[4] N. Jiao, W. Liu, T. Meng, J. Peng, and S. Mao, "Design and control of a two-phase brushless exciter for aircraft wound-rotor synchronous starter/generator in the starting mode," Power Electronics, IEEE Transactions on, vol. 31, pp. 4452-4461, 2016.

[5] J. Wei, Q.Zheng, M. Shi, B. Zhou, and J. Li, "The excitation control strategy of the three-stage synchronous machine in the start mode," in Applied Power Electronics Conference and Exposition (APEC), 2014 IEEE, 2014, pp. 2469-2474.

[6] N. Jiao, W. Liu, T. Meng, J. Peng, and S. Mao, "Research on excitation control methods for the two-phase brushless exciter of wound-rotor synchronous starter/generators in the starting mode," in Applied Power Electronics Conference and Exposition (APEC), 2016 IEEE, 2016, pp. 2776-2781.

[7] A. Griffo, D. Drury, T. Sawata, and P. H. Mellor, "Sensorless starting of a wound-field synchronous starter/generator for aerospace applications," Industrial Electronics, IEEE Transactions on, vol. 59, pp. 3579-3587, 2012.

[8] A. Maalouf, L. Idkhajine, S. Le Ballois, and E. Monmasson, "Field programmable gate array-based sensorless control of a brushless synchronous starter generator for aircraft application," Electric Power Applications, IET, vol. 5, pp. 181-192, 2011.

[9] J. Peng, W. Liu, J. Meng, T. Meng, G. Luo, "Initial orientation and sensorless starting strategy of Wound-Rotor Synchronous Starter/Generator," in Applied Power Electronics Conference and Exposition (APEC), 2016 IEEE, 2016, pp. 2748-2753.

[10] A. Markunas, "Sensorless rotor position determination for a wound field synchronous machine": US, US 20130193888 A1[P]. 2013.

[11] C. Hasegawa1 and S. Nishikata1, "A sensorless rotor position detecting method for self-controlled synchronous motors," in Electrical Machines and Systems, 2008, ICEMS 2008, International Conference on, pp. 1017-1021.

[12] J. Choi, I. Jeong, K. Nam and S. Jung, "Sensorless Control for Electrically Energized Synchronous Motor Based on Signal Injection to Field Winding," in Industrial Electronics Society, IECON 2013 - 39th Annual Conference of the IEEE, pp 3120-3129.

[13] A. Rambetius, S. Ebersberger, M. Seilmeier and B. Piepenbreier, "Carrier signal based sensorless control of electrically excited synchronous machines at standstill and low speed using the rotor winding as a receiver," Power Electronics and Applications (EPE), 2013 15th European Conference on, pp. 1-10.

[14] S. Feuersänger M. Pacas, "Rotor Position Identification in Synchronous Machinesby Using the Excitation Machine as a Sensor," Sensorless Control for Electrical Drives (SLED), 2016 IEEE Symposium on, 2016, pp. 1-6.